■ **Organic & Supramolecular Chemistry**

The Role of a Nitro Substituent in *C*-Phenylcalix[4]resorcinarenes to Enhance the Adsorption of Gold(III) Ions

Krisfian Tata Aneka Priyangga,[a] Yehezkiel Steven Kurniawan,[a] and Leny Yuliati*[a, b]

Nitro-substituted *C*-phenylcalix[4]resorcinarene derivatives were synthesized and evaluated for gold(III) ions adsorption. All the nitro-substituted *C*-phenylcalix[4]resorcinarenes showed higher maximum adsorption capacity as compared to the bare *C*-phenylcalix[4]resorcinarene. A remarkable high adsorption capacity of up to 272.70 mg g^{-1} was obtained after 2 h on the *C*-2-nitrophenylcalix[4]resorcinarene (Calix-2NO$_2$), which was two times higher than that of the *C*-phenylcalix[4]resorcinarene. The adsorption capacity was affected by the position of the nitro group. The highest adsorption capacity observed on the Calix-2NO$_2$ was closely related to the strongest supramolecular interactions between the gold(III) ions and the Calix-2NO$_2$, as supported by Fourier transform infrared (FTIR) and proton nuclear magnetic resonance (^{1}H-NMR) spectroscopies as well as the desorption study. This study demonstrated that the macrocyclic material, namely nitro-substituted *C*-phenylcalix[4]resorcinarenes, were effective adsorbents having good reusability, and thus, applicable for gold(III) ions recovery.

Introduction

Gold is one of the precious metals which is greatly used in jewelry, electronics, smart material, and advanced technologies[1,2] owing to its unique physicochemical properties as compared to other precious metals.[3] The consequence of the excessive usage of gold making its source is kept depleting by days.[4,5] Commonly found as gold(III) ions, its recovery from urban mine may act as an untapped resource in the future.[6,7] Conventional methods for gold(III) ions recovery are adsorption, solvent extraction, chemical precipitation, and membrane filtration.[8–11] Among these methods, the adsorption method is attractive as it is cheap, simple, and could be performed in the absence of toxic organic solvents.[12]

Many adsorbents for gold(III) ions have been developed such as activated carbon,[13] polyethyleneimine,[14] montmorillonite,[15] and hybrid biosorbent.[16] Activated carbon, unfortunately, only gave 9.95 mg g^{-1} as its maximum adsorption capacity (*qm*) after a very long equilibrium time of 24 h.[13] On the other hand, the polyethyleneimine gave a higher *qm* value of 286 mg g^{-1} after 6 h-shaking,[14] which is still a time-consuming process. Even though the montmorillonite composite material gave a faster equilibrium time of 1.5 h, the poor *qm* value of 1.49 mg g^{-1}[15] made this material far from the application. On the other hand, a biosorbent material containing tannin acid immobilized dialdehyde corn starch was reported to give a high *qm* value of 298.50 mg g^{-1}, but the equilibrium time was still quite long, which was 6 h.[16] Employing adsorbent materials having high adsorption capacity and short equilibrium time would be a great benefit and this leaves a great challenge for the researchers.
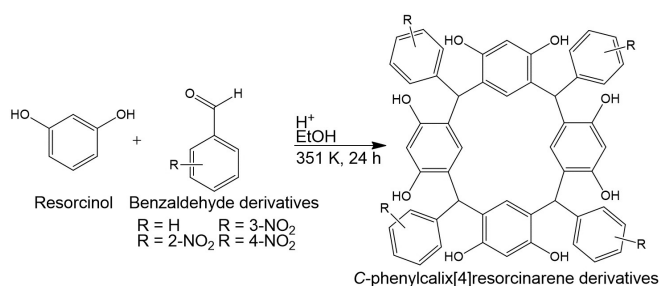
Macrocyclic organic compounds have been known for their outstanding adsorption capability due to their strong host-guest interactions.[17,18] Particular attention is on calix[n]resorcinarenes that can be prepared from a one-pot reaction between resorcinol and aldehyde compounds in acidic conditions.[19,20] The calix[4]resorcinarene derivatives have good physical properties such as high chemical stability, high thermal stability, poor solubility in aqueous media, and relatively low toxicity.[21,22] All these good properties make them suitable candidates for metal ion adsorption. *C*-phenylcalix[4]resorcinarene is considered as a simple calix[4]resorcinarene derivative having eight benzene rings and eight hydroxyl groups exhibiting good capability for heavy metal adsorption.[21,23,24] The hydroxyl groups and the aromatic rings provide binding sites for both hard and soft acids such as lead(II) and chromium(III) ions.[19] However, to the best of our knowledge, the application of calix[4]resorcinarene for gold(III) ions adsorption has not been yet reported.

Since the addition of heteroatom substituents such as −N and −O groups[25] may enhance the adsorption capacity of calix[4]resorcinarene toward gold(III) ions, three compounds of nitro-substituted *C*-phenylcalix[4]resorcinarene derivatives, *i.e.* *C*-2-nitrophenylcalix[4]resorcinarene (Calix-2NO$_2$), *C*-3-nitrophenylcalix[4]resorcinarene (Calix-3NO$_2$), and *C*-4-nitrophenylcalix[4]resorcinarene (Calix-4NO$_2$) were synthesized from resorcinol and nitrobenzaldehyde. The maximum adsorption capacity towards gold(III) ions, as well as the adsorption kinetics and thermodynamics, were investigated. The importance of nitro

[a] *K. T. A. Priyangga, Y. S. Kurniawan, Dr. L. Yuliati*
Ma Chung Research Center for Photosynthetic Pigments
Universitas Ma Chung
Villa Puncak Tidar N-01, Malang 65151, East Java, Indonesia
E-mail: leny.yuliati@machung.ac.id
[b] *Dr. L. Yuliati*
Department of Chemistry, Faculty of Science and Technology
Universitas Ma Chung
Villa Puncak Tidar N-01, Malang 65151, East Java, Indonesia

ChemistrySelect

Full Papers
doi.org/10.1002/slct.202101067

Chemistry Europe
European Chemical
Societies Publishing

Scheme 1. Synthesis of *C*-phenylcalix[4]resorcinarene derivatives.

group and its position to enhance the supramolecular interactions with gold(III) ions were revealed by desorption study and elucidated by Fourier transform infrared (FTIR) and proton nuclear magnetic resonance (^{1}H-NMR) spectroscopies. The reusability test was also performed on the Calix-2NO$_2$ adsorbent.

Results and Discussion

Synthesis and Characterizations

The *C*-phenylcalix[4]resorcinarene derivatives were synthesized from resorcinol and benzaldehyde or nitrobenzaldehyde compounds as starting materials. Under the acidic condition, both starting materials were reacted to form a cyclic structure of *C*-phenylcalix[4]resorcinarene as shown in Scheme 1. The *C*-phenylcalix[4]resorcinarene derivatives, *i.e.* Calix-2NO$_2$, Calix-3NO$_2$, Calix-4NO$_2$, and Calix-H were obtained in 93.5, 39.6, 48.5, and 95.5% yield, respectively.

The successful synthesis of all *C*-phenylcalix[4]resorcinarene derivatives was supported by their FTIR, ^{1}H-NMR, ^{13}C-NMR, and LC-HRMS spectra. As depicted in Figure 1, the disappearance of the C–H aldehyde peaks at 2700–2850 cm^{-1} and the appear-
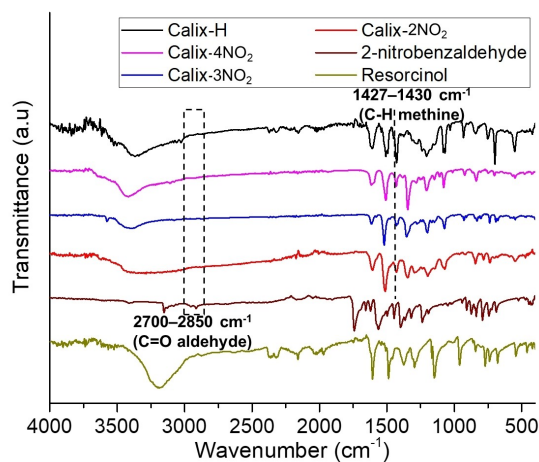
ance of the C–H methine peak of *C*-phenylcalix[4] resorcinarenes at 1427–1430 cm^{-1} indicated the successful formation of *C*-phenylcalix[4]resorcinarene and *C*-nitrophenyl-calix[4]resorcinarenes. The presence of C–H methine on *C*-phenylcalix[4]resorcinarene and *C*-nitrophenylcalix[4] resorcinarenes was also confirmed by a singlet peak at 5.27–5.37 ppm on the ^{1}H-NMR spectra and a peak at 102.6–103.4 ppm on the ^{13}C-NMR spectra, as shown in Figures S1–S4. Furthermore, the FTIR and NMR spectra of the Calix-H and the Calix-3NO$_2$ were in good agreement with the reported ones.[20,26,27] The identification of the Calix-2NO$_2$ and Calix-4NO$_2$ was also further conducted by LC-HRMS, which chromatogram and the spectra are depicted in Figures S1 and S3, respectively. The m/z of 973.00 and 973.70 as $[M+H]^+$ were obtained, further indicating the successful synthesis of these *C*-nitro-phenylcalix[4]resorcinarenes.

Adsorption for gold(III) ions

The adsorption capability of *C*-phenylcalix[4]resorsinarene derivatives was evaluated to study the effect of the nitro substituent on the adsorption of gold(III) ions. Figure 2(a) shows the dependence of adsorption percentage on the
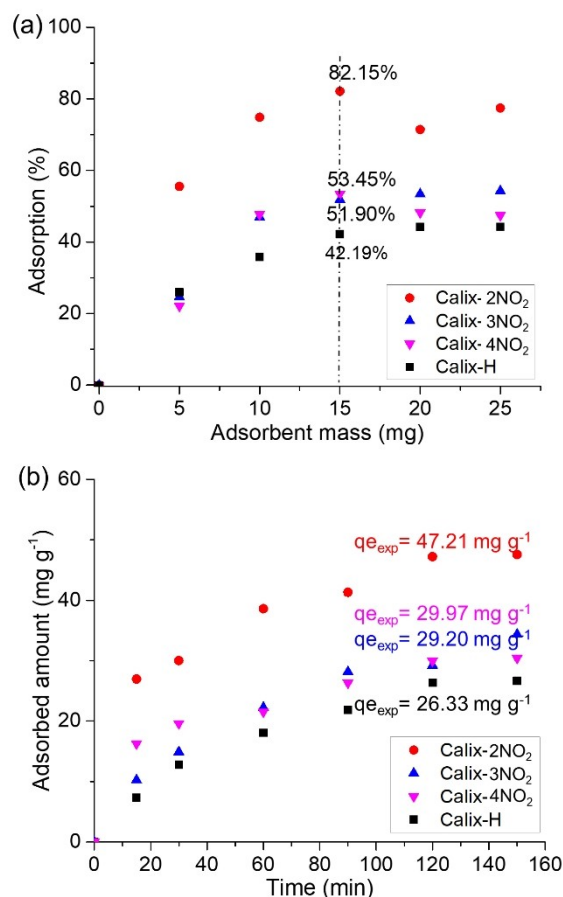

Figure 1. FTIR spectra of reactants and all the synthesized *C*-phenylcalix[4]-resorcinarene derivatives.

Figure 2. Effect of adsorbent mass (a) and time (b) on the adsorption of gold(III) ions using *C*-phenylcalix[4]resorcinarene derivatives.

ChemistrySelect

Full Papers
doi.org/10.1002/slct.202101067

**Chemistry
Europe**
European Chemical
Societies Publishing

amount of the adsorbent after 2 h-stirring. The adsorption percentage increased with the amount of adsorbent up to 15 mg on all the *C*-phenylcalix[4]resorsinarene derivatives. A further increase was not observed when the adsorbent amount was set to a higher amount, suggesting that 15 mg of adsorbent was enough to adsorb the gold(III) ions. It was noted that all the nitro-substituted *C*-phenylcalix[4]resorcinarenes gave a larger value of adsorption percentage as compared to the non-substituted one, with the order of Calix-2NO$_2$ > Calix-3NO$_2$ ≈ Calix-4NO$_2$ > Calix-H.

Using the optimum mass of adsorbent (15 mg), the adsorption was examined under different contact times. The results are shown in Figure 2(b). The amount of adsorbed gold(III) ions increased with the increase of the contact time up to 120 min, suggesting that the equilibrium time was achieved after 120 min. The Calix-2NO$_2$ gave the highest adsorbed amount of gold(III) ions at the equilibrium (qe_{exp}) which value of 47.21 mg g^{-1}, followed by the Calix-3NO$_2$ and Calix-4NO$_2$, which gave 29.20 and 29.97 mg g^{-1}, respectively. The nitro-substituted *C*-phenylcalix[4]resorcinarenes showed higher qe_{exp} values than the Calix-H, which only gave 26.33 mg g^{-1}.

Isotherm adsorption was studied by varying the initial concentration of gold(III) ions. The dependence of initial concentration on the adsorbed amount of gold(III) ions is depicted in Figure 3. The maximum adsorption capacity (qm_{exp}) values of Calix-2NO$_2$, Calix-3NO$_2$, Calix-4NO$_2$, and Calix-H were confirmed to be 272.70, 163.00, 143.86, and 129.84 mg g^{-1}, respectively. To describe the isotherm adsorption in more detail, Langmuir and Freundlich models were employed in the calculation. While the obtained data did not give linear Freundlich plots, the adsorption of gold(III) ions fitted well the Langmuir isotherm model as shown in Figure S5 and Table S1. Since the process followed the Langmuir plot, the adsorption would occur through a chemical interaction (chemisorption) rather than physical adsorption (physisorption).

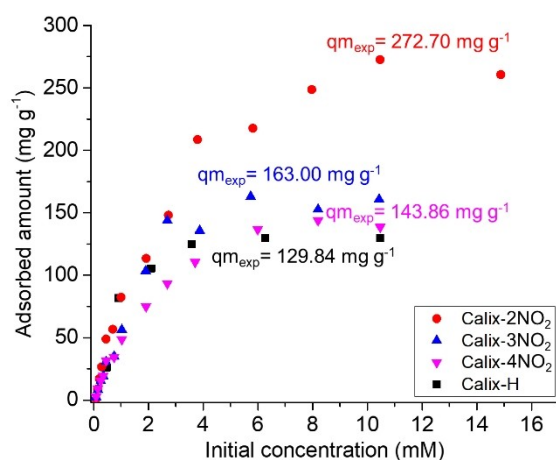The calculated maximum adsorption capacity (qm_{calc}), the Langmuir constant (K_L), the equilibrium parameter (R_L), and the coefficient of determination (R^2) for Langmuir plots are listed in Table 1. The qm_{calc} values of Calix-2NO$_2$, Calix-3NO$_2$, Calix-4NO$_2$, and Calix-H were 286.95, 178.41, 167.97, and 138.99 mg g^{-1}, respectively. It was obvious that these qm_{calc} values were very similar to those of the real uptake values (qm_{exp}). Besides, taking the initial concentration of 0.5 mM, the R_L values were confirmed in the range of 0.51–0.75, suggesting that the gold(III) ions adsorption on all adsorbents was a favorable process.

Good adsorbents can be evaluated from some parameters, such as the high maximum capacity of adsorption as well as the short equilibrium time. Table 2 lists the comparison of these two parameters on several reported adsorbents and the prepared adsorbents in this work. The Calix-2NO$_2$ showed a remarkably higher maximum adsorption capacity (272.70 mg g^{-1}) than other adsorbent materials, including those functionalized by thiourea and thiol groups.[29,31–33] Even though the Calix-2NO$_2$ gave a similar level of adsorption capacity to those of the reported polyethyleneimine[14] and bisorbent-tannin acid immobilized dialdehyde corn starch,[16] the Calix-2NO$_2$ required a much shorter equilibrium time (2 h) than either the polyethylene imine (6 h)[14] or the biosorbent-tannin acid immobilized dialdehyde corn starch (12 h),[16] highlighting the potential use of the Calix-2NO$_2$ as a good adsorbent for the gold(III) ions.

Kinetics and thermodynamic studies

The kinetics of gold(III) ions adsorption was examined by four kinetic models, namely first order, second order, pseudo-first-order, and pseudo-second-order adsorption. As listed in Table 3, most of the *C*-phenylcalix[4]resorcinarene adsorbents gave better R^2 value for the pseudo-second-order adsorption than other kinetics models. As the adsorption process of gold(III) ions followed the pseudo-second-order kinetic model, the rate-determining step for gold(III) ions adsorption would be the surface adsorption onto *C*-phenylcalix[4]resorcinarene adsorbents.[28,34] This could involve the surface interactions of the hydroxyl and nitro functional groups of *C*-phenylcalix[4] resorcinarene with gold(III) ions. This adsorption model was also proposed for other metal ion adsorption on carbon nanotube adsorbent.[35]

Figure 3. Isotherm adsorption of gold(III) ions on the *C*-phenylcalix[4]resorcinarene derivatives.

Table 1. Langmuir parameters of gold(III) ions adsorption on *C*-phenylcalix-[4]resorcinarene derivatives.

Adsorbent	qm_{calc} (mg g^{-1})[a]	K_L (L mg^{-1})[b]	R_L[c]	R^2
Calix-2NO$_2$	286.95	4.71×10^{-3}	0.68	0.9949
Calix-3NO$_2$	178.41	5.31×10^{-3}	0.66	0.9936
Calix-4NO$_2$	167.97	3.30×10^{-3}	0.75	0.9930
Calix-H	138.99	9.78×10^{-3}	0.51	0.9904

[a] qm_{calc} value was calculated from the inversed slope of a linear Langmuir plot (see Table S1 for Langmuir equation). [b] K_L was obtained from the Langmuir plot (see Table S1 for Langmuir equation). [c] R_L value was calculated from the inversed value of $1 + (K_L \times Co)$.

ChemistrySelect

Full Papers
doi.org/10.1002/slct.202101067

Chemistry Europe
European Chemical
Societies Publishing

Adsorbent	Adsorbent amount (g L^{-1})	Contact time (min)	qm_{exp} (mg g^{-1})	Reference
Calcined gibsite	0.40	1440	12.00	[7]
Activated carbon	1.28	360	9.95	[13]
Polyethylene imine	1.00	90	286.00	[14]
Montmorillonite/alginate composite	100	720	1.49	[15]
Tannin acid immobilized dialdehyde corn starch	0.83	120	298.50	[16]
Clay mineral composite	40.0	60	108.30	[28]
Thiourea modified magnetite nanoparticle	1.50	400	118.46	[29]
Mesoporous silica adsorbent	1.00	120	78.80	[30]
Thiol-cotton fiber	2.0	n.a.	68.00	[31]
Thiol-functionalized Fe$_3$O$_4$@SiO$_2$ microspheres	1.50	220	43.70	[32]
Thiol-ene hydrogel	5.0	120	45.19	[33]
Calix-2NO$_2$	1.50	120	272.70	Present work
Calix-3NO$_2$	1.50	120	163.00	Present work
Calix-4NO$_2$	1.50	120	143.86	Present work
Calix-H	1.50	1440	129.84	Present work

Table 2. Comparison of adsorption capability towards gold(III) ions using several adsorbent materials.

Table 3. Kinetic and adsorption diffusion models of gold(III) adsorption using *C*-phenylcalix[4]resorcinarene derivatives.

Model	Equation	R^2			
		Calix-2NO$_2$	Calix-3NO$_2$	Calix-4NO$_2$	Calix-H
Kinetic Models					
First order	ln $qt = -k\ t + $ ln qo	0.9825	0.9546	0.9650	0.9859
Second order	$1/qt = k\ t + 1/qo$	0.9208	0.9656	0.9642	0.9930
Pseudo first order	ln $(qe-qt) = $ ln $qe-k\ t$	0.9059	0.9761	0.9168	0.9972
	$t/qt = 1/kqe^{-2} + t/qe$	0.9921	0.9817	0.9806	0.9908
	qe_{calc} (mg g^{-1})	48.24	31.36	30.50	29.95
Pseudo second order	qe_{exp} (mg g^{-1})	47.21	29.20	29.97	26.33
	k (g mg^{-1} min^{-1})	1.98×10^{-3}	1.61×10^{-3}	1.59×10^{-3}	1.14×10^{-3}
Adsorption Diffusion Models					
Intraparticle diffusion	$qt = k\ t^{-0.5} + C$	0.9273	0.9938	0.9405	0.9901
	k (mg g^{-1} min$^{-0.5}$)	3.71	2.81	2.37	2.32
Liquid film diffusion	ln $(1-qt/qe) = -k\ t$	0.9829	0.9761	0.9280	0.8449

Based on the linear plots of the pseudo-second-order model, the amount of adsorbed gold(III) ions in equilibrium could be calculated (qe_{calc}). It was confirmed that the qe values obtained from the experimental and the calculated ones were at a similar level to each other, suggesting that the proposed kinetic model was suitable to explain the adsorption process. The adsorption rate constants (k) were determined from the pseudo-second-order model and the values are also listed in Table 3. It was obtained that the k values of the *C*-nitro-phenylcalix[4]resorcinarenes were higher than that of the Calix-H. Besides having the highest maximum adsorption capacity, the Calix-2NO$_2$ also showed the fastest adsorption rate towards gold(III) ions.

To understand the diffusion model in gold(III) ions adsorption, two types of adsorption diffusion models were examined, which were intraparticle and liquid film diffusions. The equations used and the R^2 values for each model could be seen in Table 3. In general, the adsorption data were better fitted to the intraparticle than the liquid film diffusion model.

This result showed that the adsorption of gold(III) ions onto the *C*-phenylcalix[4]resorcinarene materials was a diffusion-controlled process. Since the adsorption data fitted the pseudo-second-order and intraparticle diffusion, the overall rate-determining step could be complex.[36] As the trend of the calculated adsorption constant rate (k) values employing this intraparticle diffusion model were similar to that of the pseudo-second-order kinetic model, the adsorption rate would be strongly affected by the diffusion-controlled process.

The thermodynamic parameters such as enthalpy change (ΔH), Gibbs energy change (ΔG), and entropy change (ΔS) values of the gold(III) ions adsorption were investigated on the *C*-phenylcalix[4]resorcinarenes by varying the adsorption temperatures. The correlation between these parameters can be determined according to the following equations (1)–(4), whereas K is the equilibrium constant, C_s is the concentration of gold(III) in the *C*-phenylcalix[4]arenes after adsorption (mM), C_e is the equilibrium concentration of gold(III) ions in the

ChemistrySelect

Full Papers
doi.org/10.1002/slct.202101067

Chemistry
Europe
European Chemical
Societies Publishing

aqueous solution (mM), R is the gas constant (8.314 J mol^{-1} K^{-1}), and T is the adsorption temperature (K).[7,37]

$$K = C_s/C_e \tag{1}$$

$$d\ln K/d(1/T) = -\Delta H/R \tag{2}$$

$$\Delta G = -RT \ln K \tag{3}$$

$$\ln K = \Delta S/R - \Delta H/RT \tag{4}$$

The calculated thermodynamic parameters are listed in Table 4. The gold(III) ions adsorption on all the *C*-phenylcalix[4]resorcinarenes was shown to be an exothermic process ($\Delta H < 0$). The ΔH value can be used to indicate whether the adsorption is physisorption (-4 to -40 kJ mol^{-1}) or chemisorption (-40 to -800 kJ mol^{-1}).[38] Since the ΔH values were in the range of -52.50 to -94.50 kJ mol^{-1}, the gold(III) ions adsorption occurred through a chemisorption process, in good agreement with the linear Langmuir plot discussed previously. Since the ΔH value of Calix-2NO$_2$ was much lower than those of the Calix-3NO$_2$ and the Calix-4NO$_2$, the chemical interactions between gold(III) ions and Calix-2NO$_2$ adsorbent would be much stronger than those that occurred on the Calix-3NO$_2$ and the Calix-4NO$_2$. The stronger interaction would lead to the larger adsorbed amount of gold(III) ions, which could be also indicated from the larger qe_{exp} and qm_{exp} values, whereas the order was Calix-2NO$_2 >$ Calix-3NO$_2 \approx$ Calix-4NO$_2$.

The ΔG values were in the range of -10 to -13 kJ mol^{-1}, indicating that the gold(III) ions adsorption on *C*-phenylcalix[4]resorcinarene derivatives occurred spontaneously. Increasing the adsorption temperature resulted in a lower amount of adsorbed gold(III) ions as the adsorption-desorption equilibrium would be affected. A similar effect in the adsorption process was reported in which the increased temperature led to a decrease in adsorption driving force.[39] Therefore, a temperature of 298 K was the most preferable temperature to obtain the highest gold(III) ions adsorption. All the *C*-phenylcalix[4]resorcinarene derivatives gave negative ΔS values, implying that the randomness was decreased in the solid-solution interface during the adsorption process, which was similar to the previous report.[37] Again the ΔS value on the Calix-2NO$_2$ was more negative than the other adsorbents,

suggesting that the least disordered adsorption occurred on the Calix-2NO$_2$.

Effect of nitro group position

As shown previously, the nitro substituent (-NO$_2$) enhanced the adsorption capability of the *C*-phenylcalix[4]resorcinarene framework, where the order was Calix-2NO$_2 >$ Calix-3NO$_2 \approx$ Calix-4NO$_2 >$ Calix-H. To elucidate the reasons for such a result, spectroscopic studies using FTIR and ^{1}H-NMR were performed to compare the adsorbent materials before and after the adsorption process. The FTIR spectra of all *C*-phenylcalix[4]resorcinarene derivatives before and after the gold(III) ions adsorption are shown in Figure 4. The stretching vibration of the hydroxyl group (-OH$_{str}$) of *C*-phenylcalix[4]resorcinarenes could be observed around 3372.8–3428.8 cm^{-1}. The vibration peaks were shifted to a higher wavenumber at 3401.8–3447.1 cm^{-1} after the adsorption of gold(III) ions. When the gold(III) ions were adsorbed on *C*-phenylcalix[4]resorcinarene, the partially negative oxygen atom in the hydroxyl group could form electrostatic interactions to the gold(III) ions, forming the gold(III)-calix complex. Such interactions would lead to the disturbance on the intramolecular hydrogen bonding of *C*-phenylcalix[4]resorcinarene. Therefore, it was reasonable to observe the shifting of the -OH$_{str}$ signals to a higher wavenumber region. The shifting difference of each *C*-phenylcalix[4]resorcinarene derivative before and after the adsorption process was calculated. It was found that the difference in -OH$_{str}$ stretching wavenumbers for Calix-2NO$_2$, Calix-3NO$_2$, and Calix-4NO$_2$ were 41.5, 29.0, and 18.3 cm^{-1}, respectively. This result suggested that the strongest electrostatic interactions occurred between the gold(III) ions and the Calix-2NO$_2$. Furthermore, the stretching signal of the –NO$_2$ group in *C*-phenylcalix[4]resorcinarene was also shifted to a higher wavenumber caused by the intramolecular interactions between the –NO$_2$ groups and the gold(III) ions. It was found that the difference in -NO$_2$ stretching wavenumbers for Calix-2NO$_2$,
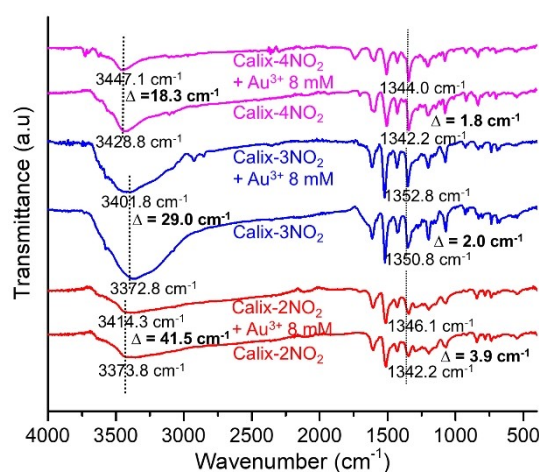
Table 4. Thermodynamic parameters on the gold(III) adsorption of using *C*-nitrophenylcalix[4]resorcinarenes at different adsorption temperatures.

Adsorbent	T (K)	ΔH (kJ mol^{-1})	ΔG (kJ mol^{-1})	ΔS (J mol^{-1} K^{-1})
	298		−13.37	−272.2
Calix-2NO$_2$	303	−94.50	−11.64	−273.5
	308		−10.65	−272.2
	298		−12.27	−136.5
Calix-3NO$_2$	303	−52.96	−11.47	−136.9
	308		−10.91	−136.5
	298		−12.37	−134.7
Calix-4NO$_2$	303	−52.50	−11.55	−135.1
	308		−11.02	−134.7

Figure 4. FTIR spectra of *C*-nitrophenylcalix[4]resorcinarene adsorbents before and after adsorption of gold(III) ions.

ChemistrySelect

Full Papers
doi.org/10.1002/slct.202101067

Chemistry Europe
European Chemical
Societies Publishing

Calix-3NO$_2$, and Calix-4NO$_2$ were 3.9, 2.0, and 1.8 cm^{-1}, respectively. This result indicated that the —NO$_2$ group facilitated the gold(III) ions adsorption.

To further clarify the supramolecular interactions above, the ^{1}H-NMR spectra of Calix-2NO$_2$ before and after the gold(III) ions adsorption were recorded and shown in Figure 5. The Calix-2NO$_2$ was used as the representative adsorbent as it exhibited the highest adsorption capacity for gold(III) ions. It was obvious that the proton signals from the —OH group in Calix-2NO$_2$ were simplified to be a broad singlet and shifted to the downfield from 9.0 to 8.75 ppm after the gold(III) ions adsorption. This result suggested that some of the —OH groups could be deprotonated due to electrostatic interaction with gold(III) ions.[40] Meanwhile, the weakened hydrogen bonding would lead to the downfield shifting. In addition, the aromatic rings of Calix-2NO$_2$ after gold(III) ions adsorption were confirmed to be more ordered than before the adsorption, indicating the formation of a more rigid conformation as the result of the interactions in the gold(III)-calix complex. The aromatic proton signals of free Calix-2NO$_2$ were found as multiplet which attributed to the mobile conformation of the Calix-2NO$_2$. In contrast, the aromatic proton signals of gold(III)-calix complex was simpler and sharper, which suggested that the gold(III) ions locked the Calix-2NO$_2$ in cone conformation due to cation-π interactions as previously reported.[41] The merging of the —CH$_2$ proton signal from the methine bridge was also observed that also supported the existence of gold(III)-calix in cone conformation.

It was demonstrated that the position of nitro substituent affected the adsorption capacity of the Calix-H differently. As for the Calix-2NO$_2$, the —NO$_2$ group was in ortho position which was very close to the position of the hydroxyl group in calix[4]resorcinarene framework. This position would create a strong stabilization inductive effect, giving the high complexation energy to form gold(III)-calix complex. As a result, the stronger interaction would lead to a higher adsorption capability. Since the —NO$_2$ group of the Calix-3NO$_2$ and the Calix-4NO$_2$ was located at meta and para position, weaker complexation energy of gold(III)-calix was generated, yielding a lower q_m value than the Calix-2NO$_2$ but higher than the Calix-H.
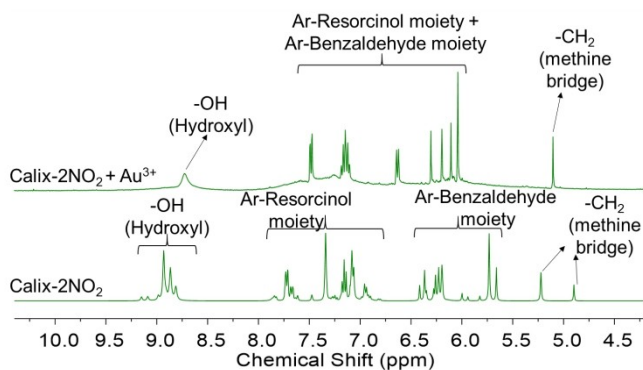
Desorption of gold(III) ions and reusability test

The calculated complexation energy as well as the FTIR and ^{1}H-NMR spectra revealed that among the C-phenylcalix[4]resorcinarene derivatives, the Calix-2NO$_2$ has the strongest supramolecular interactions towards gold(III) ions. A further study was conducted to desorb the gold(III) ions that were adsorbed onto C-nitrophenylcalix[4]resorcinarenes with the help of an acidic solution. It was obtained that the desorption of gold(III) ions were 7.36, 8.20, and 14.14 mg g^{-1} or 15.58, 28.09, and 47.18% for Calix-2NO$_2$, Calix-3NO$_2$, and Calix-4NO$_2$, respectively, when using HCl 0.1 M after 2 h-contact time. Among the C-nitrophenylcalix[4]resorcinarenes, the Calix-2NO$_2$ gave the lowest amount of desorbed gold(III) ions, again indicating the strongest interactions of the Calix-2NO$_2$ towards the gold(III) ions.

The desorption percentage of gold(III) ions from the Calix-2NO$_2$ could be improved further when employing an acidic solution with greater concentration or stronger acidity. Increasing the HCl concentration from 0.1 to 1.0 M slightly increased the desorption percentage from 15.58 to 20.02%. By using stronger acid reagents, i.e. 1.0 M HNO$_3$ and 1.0 M H$_2$SO$_4$, higher desorption percentages were achieved as high as 25.18 and 31.22%, respectively. Since the acidic solution treatment could not desorb completely the gold(III) ions, another desorption process was employed. It was reported that the acidic conditions could lead to the reduction of gold(III) ions to gold(0).[42–44] Such reduction mechanism was also reported in the adsorption of gold(III) ions on the tannin acid immobilized dialdehyde corn starch.[16] Therefore, the possibility that C-phenylcalix[4]resorcinarene mediated partially the reduction of gold(III) under acidic conditions could not be excluded. Since H$_2$O$_2$ has been reported to increase the rate of Au oxidation and metallurgical Au recovery,[45,46] H$_2$O$_2$ was used to leach out the reduced gold(III) from the Calix-2NO$_2$ via the oxidation process. It was confirmed that additional gold(III) desorption was achieved (69.28%), giving a successful completion of gold(III) desorption from the Calix-2NO$_2$. Comparison to thiol-functionalized adsorbent,[31] the desorption process on the Calix-2NO$_2$ was milder as thermal process and highly concentrated acid solutions were not required.

The gold(III)-free Calix-2NO$_2$ adsorbent was then reused for the adsorption of gold(III) ions up to three cycles. Each adsorption process was followed by the desorption treatments stated above. After three cycles, the adsorption of gold(III) ions on the Calix-2NO$_2$ was mostly at the same level of 82.15, 77.41, and 75.10%. The desorption of gold(III) ions reached ~100% after each cycle. Furthermore, the structure of Calix-2NO$_2$ was not significantly changed after reusing it for three cycles as shown from the FTIR and DR UV-vis data in Figures S6 and S7, respectively. All these results indicated the stability and the potential capability of the Calix-2NO$_2$ to be employed in gold(III) recovery process.

Figure 5. ^{1}H-NMR spectra of Calix-2NO$_2$ before and after adsorption of gold(III) ions.

ChemistrySelect

Full Papers
doi.org/10.1002/slct.202101067

Chemistry Europe
European Chemical
Societies Publishing

Proposed supramolecular interactions between gold(III) ions and *C*-phenylcalix[4]resorcinarene derivatives

Since the adsorption of gold(III) ions using *C*-phenylcalix[4]resorcinarene derivatives happened through a chemisorption process, the interactions between gold(III) ions and the *C*-phenylcalix[4]resorcinarene could occur through the formation of gold(III)-calix complex. Our experimental data showed that the existence of the —NO_2 group at ortho (Calix-2NO_2), meta (Calix-3NO_2), and para (Calix-4NO_2) positions enhanced the adsorption capability of the Calix-H adsorbent. The —NO_2 group at the *C*-phenylcalix[4]resorcinarene framework would interact with gold(III) ions as its oxygen atoms have a partial negative charge. Moreover, the spectroscopic study confirmed that the hydroxyl groups interacted with gold(III) ions through electrostatic interactions. All these results suggested that the gold(III) ions would interact better when the position of the —NO_2 group is closer to —OH or in other words when the —NO_2 group is in the ortho position.

As the *C*-phenylcalix[4]resorcinarene has been recognized to have a cavity to trap metal ions through cation-π interaction,[47–49] the possibility to form the gold(III)-calix complex inside the calix cavity could not be neglected. This would give us at least two possibilities to form the gold(III)-calix complex, *i.e.*, outside the calix cavity and/or inside the calix cavity. The plausible interactions between the gold(III) ions and the Calix-2NO_2 are then proposed in Figure 6. The complex structure was proposed considering the cone conformation of calix as supported by its ^{1}H-NMR spectrum.

Conclusion

Three types of nitro-substituted *C*-phenylcalix[4]resorcinarenes were successfully synthesized with the yield of 39.6–95.5% through a single-step reaction. The optimum amount, contact time, and temperature for gold(III) ions adsorption on all the *C*-phenylcalix[4]resorcinarene adsorbents were 15 mg, 120 min, and 298 K, respectively. Under the optimum conditions, the qm_{exp} values for gold(III) adsorption on the Calix-2NO_2, the Calix-3NO_2, the Calix-4NO_2, and the Calix-H were obtained as 272.70, 163.00, 143.86, and 129.84 mg g^{-1}, respectively. The gold(III) ions adsorption process fitted well the Langmuir plot and it was shown as a favorable process on all adsorbents. The kinetic study revealed that the gold(III) ions adsorption followed the pseudo-second-order kinetic model and could occur through the intraparticle diffusion mechanism. The thermodynamic parameters indicated that the adsorption occurred more on Calix-2NO_2 due to the higher exothermic enthalpy energy, as also supported by its spontaneous process and less disordered entropy. From the spectroscopic studies, it was revealed that the gold(III) ions interacted with both hydroxyl and nitro groups as well as aromatic rings of *C*-phenylcalix[4]resorcinarene derivatives through electrostatic and cation-π interactions. Furthermore, when the -NO_2 group was located closer to calix[4]resorcinarene cavity, the gold(III) ions could be adsorbed stronger, resulting in the adsorption capability was also in the order of Calix-2NO_2 > Calix-3NO_2 ≈ Calix-4NO_2 > Calix-H. The reusability test demonstrated that the Calix-2NO_2 can be applied to the recovery of gold(III) ions.

Supporting Information Summary

Supporting Information includes the detailed experimental section, the ^{1}H-NMR, ^{13}C-NMR, LC chromatogram, and HRMS spectra of *C*-phenylcalix[4]resorcinarene derivatives, Langmuir plots for adsorption of gold(III) ions on the *C*-phenylcalix[4]-resorcinarene derivatives, the FTIR and DR UV-vis spectra of the Calix-2NO_2 before and after reusability test, as well as the coefficient determination using four adsorption models for the adsorption of gold(III) ions on the *C*-phenylcalix[4]resorcinarene derivatives.

Conflict of Interest

The authors declare no conflict of interest.

[1] R. Khosravi, A. Azizi, R. Ghaedrahmati, V. K. Gupta, S. Agarwal, *J. Ind. Eng. Chem.* **2017**, *54*, 464–471.

[2] F. Liu, S. Wang, S. Chen, *Int. J. Biol. Macromol.* **2020**, *152*, 1242–1251.

[3] C. Wang, G. Lin, J. Zhao, S. Wang, L. Zhang, *Chem. Eng. J.* **2020**, *388* 124221.

[4] B. Xu, K. Li, Z. Dong, Y. Yang, Q. Li, X. Liu, T. Jiang, *J. Cleaner Prod.* **2019**, *233*, 1475–1485.

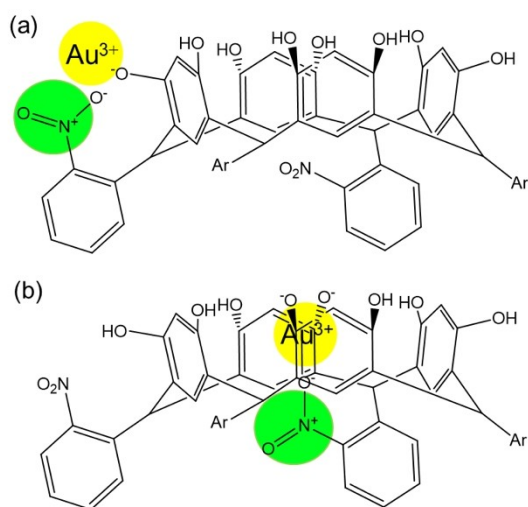**Figure 6.** Plausible formation of gold(III)-calix complex structure at the (a) outside and (b) inside of the calix cavity.

ChemistrySelect

Full Papers
doi.org/10.1002/slct.202101067

Chemistry
Europe
European Chemical
Societies Publishing

[5] S.-I. Park, I. S. Kwak, S. W. Won, Y.-S. Yun, *J. Hazard. Mater.* **2013**, *248*, 211–218.

[6] B. Xu, W. Kong, Q. Li, Y. Yang, T. Jiang, X. Liu, *Metals* **2017**, *7*, 222.

[7] F. Ogata, N. Kawasaki, *J. Chem. Eng. Data* **2014**, *59*, 412–418.

[8] Z. Reddad, C. Gerente, Y. Andres, P. L. Cloirec, *Environ. Sci. Technol.* **2002**, *36*, 2067–2073.

[9] F. J. Alguacil, P. Adeva, M. Alonso, *Gold Bull.* **2005**, *38*, 9–13.

[10] J. Baker, R. J. Baker, C. Schulzke, *Gold Bull.* **2011**, *44*, 79–83.

[11] J. Yang, F. Kubota, Y. Baba, N. Kamiya, M. Goto, *Carbohydr. Polym.* **2014**, *111*, 768–774.

[12] S. Syed, *Hydrometallurgy* **2012**, *115–116*, 30–51.

[13] P. J. Tauetsile, E. A. Oraby, J. J. Eksteen, *Sep. Purif. Technol.* **2019**, *211*, 594–601.

[14] B. C. Choudhary, D. Paul, A. U. Borse, D. J. Garole, *Sep. Purif. Technol.* **2018**, *195*, 260–270.

[15] A. Mourpichai, T. Jintakosol, W. Nitayaphat, *Mater. Today: Proc.* **2018**, *5*, 14786–14792.

[16] F. Liu, G. Peng, T. Li, G. Yu, S. Deng, *Chem. Eng. J.* **2019**, *370*, 228–236.

[17] R. R. Sathuluri, Y. S. Kurniawan, J. Y. Kim, M. Maeki, W. Iwasaki, S. Morisada, H. Kawakita, M. Miyazaki, K. Ohto, *Sep. Sci. Technol.* **2018**, *53*, 1261–1272.

[18] Y. S. Kurniawan, R. R. Sathuluri, K. Ohto, W. Iwasaki, H. Kawakita, S. Morisada, M. Miyazaki, J. Jumina, *Sep. Purif. Technol.* **2019**, *211*, 925–934.

[19] I. G. M. N. Budiana, J. Jumina, C. Anwar, *J. Appl. Chem. Sci.* **2016**, *3* 289–298.

[20] L. M. Tunstad, J. A. Tucker, E. Dalcanale, J. Weiser, J. A. Bryant, J. C. Sherman, R. C. Helgeson, C. B. Knobler, D. J. Cram, *J. Org. Chem.* **1989**, *54*, 1305–1312.

[21] J. Jumina, R. E. Sarjono, D. Siswanta, S. J. Santoso, K. Ohto, *J. Korean Chem. Soc.* **2011**, *55*, 454–462.

[22] H. M. Chawla, N. Pant, S. Kumar, S. Mrig, B. Srivastava, N. Kumar, D.StC. Black, *J. Photochem. Photobiol. B.* **2011**, *105*, 25–33.

[23] M. Tabakci, S. Erdemir, M. Yilmaz, *J. Hazard. Mater.* **2007**, *148*, 428–435.

[24] U. Rastuti, D. Siswanta, W. Pambudi, B. A. Nurohmah, B. M. Yamin, J. Jumina, *Sains Malays.* **2018**, *47*, 1167–1179.

[25] G. Lin, T. Hu, S. Wang, T. Xie, L. Zhang, S. Cheng, L. Fu, C. Xiong, *Chemosphere* **2019**, *225*, 65–72.

[26] K. T. A. Priyangga, Y. S. Kurniawan, L. Yuliati, *Iop. Conf. Ser. Mater. Sci. Eng.* **2020**, *959*, 012014.

[27] B. M. Yamin, H. M. Abosadiya, S. A. Hasbullah, J. Jumina, *Int. J. Adv. Sci. Eng. Inf. Technol.* **2014**, *4*, 125–128.

[28] Y. Rakhila, A. Elmchaouri, A. Mestari, S. Korili, M. Abouri, A. Gil, *Int. J. Miner. Metall. Mater.* **2019**, *26*, 673–680.

[29] T.-L. Lin, H.-L. Lien, *Int. J. Mol. Sci.* **2013**, *14*, 9834–9847.

[30] K. F. Lam, K. L. Yeung, G. McKay, *J. Phys. Chem. B.* **2006**, *110*, 2187–2194.

[31] M. Yu, D. Sun, W. Tian, G. Wang, W. Shen, N. Xu, *Anal. Chim. Acta* **2002**, *456*, 147–155.

[32] X. Peng, W. Zhang, L. Gai, H. Jiang, Y. Tian, *Russ. J. Phys. Chem. A* **2016**, *90*, 1656–1664.

[33] M. Fırlak, M. V. Kahraman, E. K. Yetimoğlu, *J. Appl. Polym. Sci.* **2012**, *126*, 322–332.

[34] H. Wang, A. Zhou, F. Peng, H. Yu, J. Yang, *J. Colloid Interface Sci.* **2007**, *316*, 277–283.

[35] D. Robati, *J. Nanostructure Chem.* **2013**, *3*, 55.

[36] A. Pholosi, E. B. Naidoo, A. E. Ofomaja, *S. Afr. J. Chem. Eng.* **2020**, *32*, 39–55.

[37] J. S. Piccin, G. L. Dotto, L. A. A. Pinto, *Braz. J. Chem. Eng.* **2011**, *28*, 295–304.

[38] G. Crini, P.-M. Badot, *Prog. Polym. Sci.* **2008**, *33*, 399–447.

[39] I. Uzun, F. Güzel, *J. Hazard. Mater.* **2005**, *B118*, 141–154.

[40] J. Jumina, Y. Priastomo, H. R. Setiawan, Mutmainah, Y. S. Kurniawan, K. Ohto, *J. Environ. Chem. Eng.* **2020**, *8*, 103971.

[41] J. Jumina, D. Siswanta, K. Nofiati, A. C. Imawan, Y. Priastomo, K. Ohto, *Bull. Chem. Soc. Jpn.* **2019**, *92*, 825–831.

[42] M. Luty-Błocho, K. Pacławski, M. Wojnicki, K. Fitzner, *Inorg. Chim. Acta* **2013**, *395*, 189–196.

[43] Z. Khan, T. Singh, J. I. Hussain, A. A. Hashmi, *Colloids Surf. B* **2013**, *104*, 11–17.

[44] K. Pacławski, T. Sak, *J. Min. Metall. Sect. B.* **2015**, *51*, 133–142.

[45] Q. Zhu, J. Wu, J. Zhao, W. Ni, *Langmuir* **2015**, *31*, 4072–4077.

[46] T. O. Nunan, I. L. Viana, G. C. Peixoto, H. Ernesto, D. M. Verster, J. H. Pereira, J. M. Bonfatti, L. A. C. Teixeira, *Miner. Eng.* **2017**, *108*, 67–70.

[47] A. S. Mahadevi, G. N. Sastry, *Chem. Rev.* **2013**, *113*, 2100–2138.

[48] H. Kumari, P. Jin, S. J. Teat, C. L. Barnes, S. J. Dalgarno, J. L. Atwood, *J. Am. Chem. Soc.* **2014**, *136*, 17002–17005.

[49] E. S. Español, M. M. Villamil, *Biomol.* **2019**, *9*, 90.

ChemistrySelect

WILEY-VCH
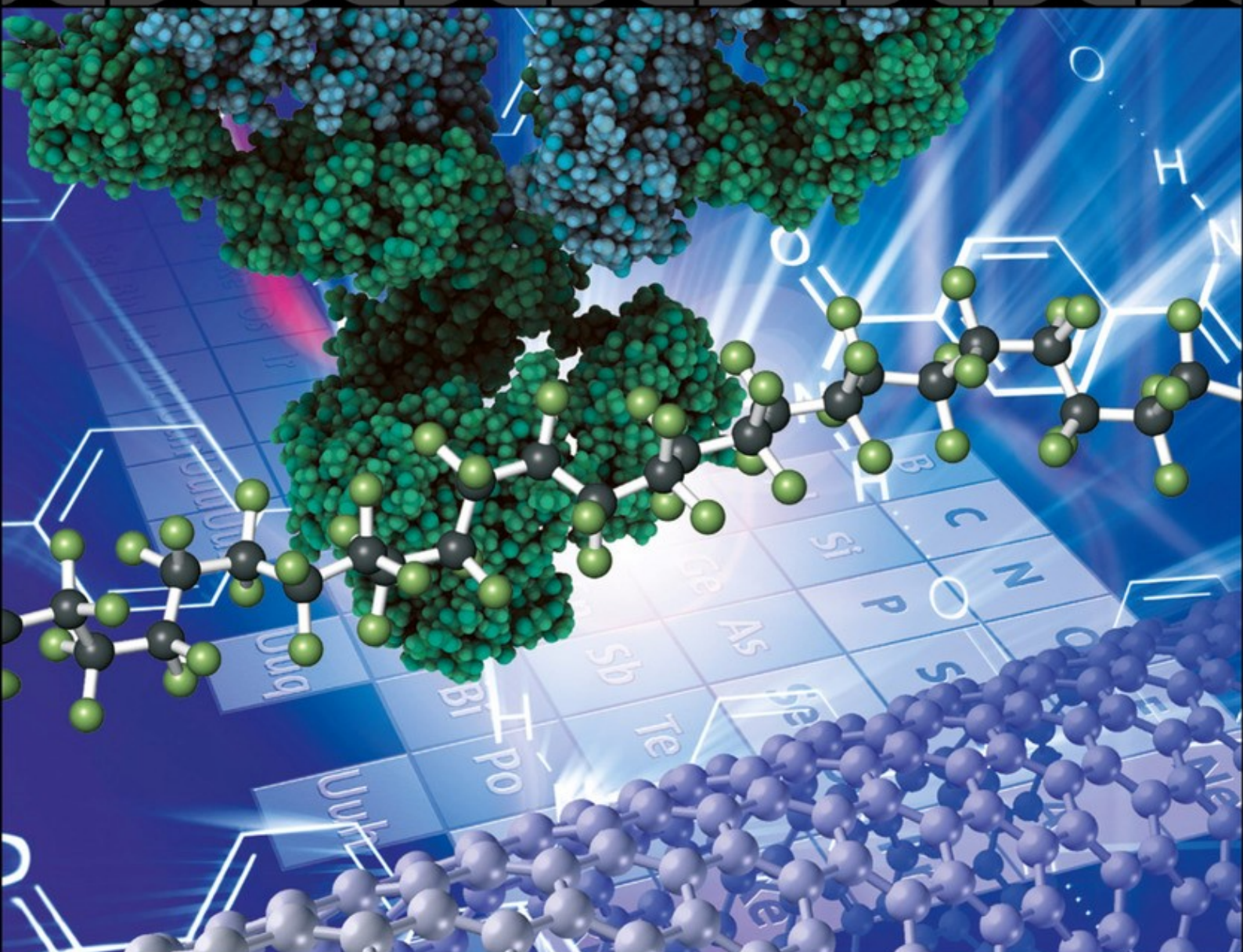
Editorial Board

Chairs

Didier Astruc is a full professor of chemistry at the Université Bordeaux I. He is known for his work on "electron-reservoir" complexes, dendritic molecular batteries, green catalysis, and sensors.

Hélène Lebel is a professor of chemistry at the Université de Montréal. Her research is focused on catalysis in synthetic organic chemistry, pharmacologically useful molecules, and multicatalytic processes that mimic biosynthesis in living cells.

An-Hui Lu is a professor of chemistry at the State Key Laboratory of Fine Chemicals, Dalian University of Technology. His research interests include the synthesis of porous materials for heterogeneous catalysis, adsorption, energy storage and conversion.

Members

- Raed **Abu-Reziq** (The Hebrew University of Jerusalem)
- Marius **Andruh** (Universitatea din Bucureşti)
- Ülkü **Anık** (Muğla Sıtkı Koçman University)
- Viktorya **Aviyente** (Boğaziçi University)
- R. Tom **Baker** (University of Ottawa)
- Thomas **Baumgartner** (York University)
- Michael J. **Bojdys** (Humboldt-Universität zu Berlin)
- Azzedine **Bousseksou** (Laboratoire de Chimie de Coordination, CNRS)
- Carlos D. **Brondino** (Universidad Nacional del Litoral)
- Juraj **Bujdak** (Univerzita Komenského v Bratislave)
- Jianfeng **Cai** (University of South Florida)
- Luigi **Cavallo** (King Abdullah University of Science and Technology)
- Jiří **Čejka** (Akademie věd České republiky)
- Hugo E. **Cerecetto** (Universidad de la República)
- Banglin **Chen** (University of Texas at San Antonio)
- Sheng **Dai** (Oak Ridge National Laboratory)
- Jiří **Damborský** (Masarykova univerzita)
- Aditi **Das** (University of Illinois)
- Fabian M. **Dayrit** (Ateneo de Manila University)
- Da-Ming **Du** (Beijing Institute of Technology)
- Charl **Faul** (University of Bristol)
- Shin-ichi **Fukuzawa** (Chuo University)
- François **Gabbaï** (Texas A&M University)
- Miran **Gaberšček** (Kemijski inštitut Ljubljana Slovenija)
- Karol **Grela** (University of Warsaw)
- Daniel **Gryko** (Polska Akademia Nauk)
- Michael **Harmata** (University of Missouri-Columbia)
- Dennis **Hetterscheid** (Universiteit Leiden)
- Yong-Sheng **Hu** (Institute of Physics, CAS)
- Reuben **Hwu** (National Tsing Hua University)
- Josef **Jampilek** (Univerzita Komenského v Bratislave)
- Hye-Young **Jang** (Ajou University)
- Deborah **Jones** (L'Institut de Chimie Moléculaire et des Matériaux)
- Babak **Karimi** (Institute for Advanced Studies in Basic Sciences)
- Uwe **Karst** (Westfälische Wilhelms-Universität Münster)
- Henryk **Kozłowski** (Uniwersytet Wrocławski)

🇺🇸 Yuehe **Lin** (Washington State University)
🇨🇳 Chenghui **Liu** (Shaanxi Normal University)
🇨🇳 Chun-yan **Liu** (Technical Institute of Physics and Chemistry, CAS)
🇸🇮 Gregor **Mali** (Kemijski inštitut Ljubljana Slovenija)
🇪🇸 Jose L. **Marco-Contelles** (Química Orgánica General del CSIQ)
🇺🇸 Sherri **McFarland** (University of North Carolina at Greensboro)
🇲🇽 Gabriel **Merino** (Centro de Investigación y de Estudios Avanzados Unidad Mérida)
🇯🇵 Kenji **Miyatake** (University of Yamanashi)
🇺🇸 Yirong **Mo** (Western Michigan University)
🇩🇪 Thomas E. **Müller** (RWTH Aachen)
🇨🇦 Samir H. **Mushrif** (University of Alberta)
🇮🇳 Srinivasan **Natarajan** (Indian Institute of Science, Bangalore)
🇨🇦 Georgii I. **Nikonov** (Brock University)
🇹🇷 Turan **Öztürk** (Istanbul Technical University)
🇮🇹 Mario **Pagliaro** (Istituto per lo Studio dei Materiali Nanostrutturati del CNR, Palermo)
🇮🇹 Maurizio **Peruzzini** (Dipartimento Scienze Chimiche e Technologie del CNR)
🇵🇹 Teresa M. V. D. **Pinho e Melo** (Universidade De Coimbra)
🇪🇸 Uwe **Pischel** (Universidad de Huelva)
🇭🇺 László **Poppe** (Budapesti Műszaki és Gazdaságtudományi Egyetem)
🇹🇭 Vinich **Promarak** (Vidyasirimedhi Institute of Science and Technology)
🇬🇧 Rasmita **Raval** (University of Liverpool)
🇮🇩 Leni **Ritmaleni** (Universitas Gadjah Mada)
🇦🇺 Johan **Rosengren** (The University of Queensland)
🇧🇷 Liane Marcia **Rossi** (Universidade de São Paulo)
🇵🇱 Agnieszka **Ruppert** (Politechnika Łódzka)
🇩🇪 Ulrich **Schatzschneider** (Julius-Maximilians-Universität Würzburg)
🇺🇸 YuYe Jay **Tong** (Georgetown University)
🇬🇷 Konstantinos S. **Triantafyllidis** (Aristotle University of Thessaloniki)
🇬🇷 Andrew **Tsotinis** (University of Athens)
🇨🇳 Xinchen **Wang** (Fuzhou University)
🇺🇸 Gang **Wu** (University at Buffalo)

Former Members

➕ Christian **Heinis** (École Polytechnique Fédérale de Lausanne)
🇩🇰 Knud **Jensen** (Københavns Universitet)
🇨🇳 Gaoquan **Shi** (Tsinghua University)

✏️ **Submit a Manuscript**

📄 **Browse free sample issue**

🔔 **Get content alerts**

✪ **Subscribe to this journal**

More from this journal

- Reviews
- Editorials
- Video Abstracts

< Previous Issue | Next Issue >

GO TO SECTION

" Export Citation(s)

Cover Pictures

Cover Picture: (21/2021)

Pages: 5166 | First Published: 01 June 2021
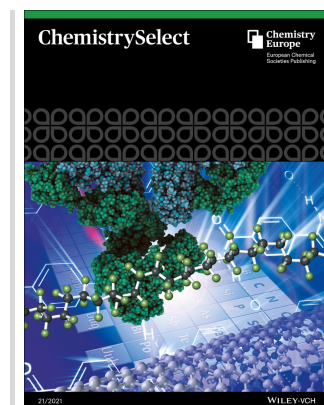
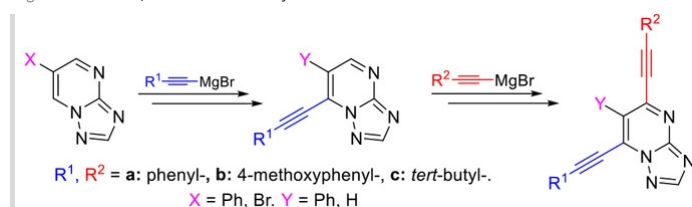Abstract | Full text | PDF | Request permissions

Full Papers

Organic & Supramolecular Chemistry

Ethynylation of [1,2,4]Triazolo[1,5-*a*]pyrimidinesUsing Substituted Ethynylmagnesium Bromides

Dr. Nikolay A. Rasputin, Dr. Nadezhda S. Demina, Dr. Ekaterina F. Zhilina, Dr. Maksim A. Averkov, Dr. Gennady L. Rusinov, Prof. Oleg N. Chupakhin, Prof. Valery N. Charushin

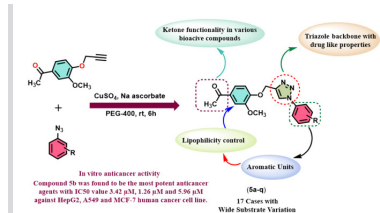Pages: 5167-5172 | First Published: 01 June 2021

$R^1, R^2 =$ **a**: phenyl-, **b**: 4-methoxyphenyl-, **c**: *tert*-butyl-.
X = Ph, Br. Y = Ph, H

A simple, transition metal-free method for the functionalization of [1,2,4]triazolo[1,5-*a*]pyrimidines has been described. Mono- and disubstituted of [1,2,4]triazolo[1,5-*a*]pyrimidines were obtained using substituted ethynylmagnesium bromides via elemination and oxidation pathways of hydrogen nucleophilic substitution. The photophysical and redox properties of the obtained compounds showed their as promising UV-dyes with high quantum yields up to 0.82

Abstract | Full text | PDF | References | Request permissions

Medicinal Chemistry & Drug Discovery

Synthesis and In Vitro Anticancer Activities of New 1,4-Disubstituted-1,2,3-triazoles Derivatives through Click Approach

Amol S. Nipate, Chetan K. Jadhav, Dr. Asha V. Chate, Dr. Tejshri R. Deshmukh, Dr. Aniket P. Sarkate, Prof. Charansingh. H. Gill

The synthesis of a new series 1-(3-methoxy-4-((1-phenyl-1H-1,2,3-triazole-4-yl)methoxy) phenyl)ethanone *via* click chemistry approach utilizing azide-alkyne cycloaddition reactions is reported in this study.

Abstract | Full text | PDF | References | Request permissions

---
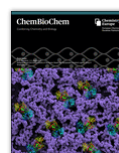
Catalysis

Effects of Mn^{II} and Eu^{III} Cation Exchange in Sepiolite-Titanium Dioxide Nanocomposites in the Photocatalytic Degradation of Orange G

Dr. Brittany A. Cymes, Dr. Alex J. Kugler, Dr. Catherine B. Almquist, Dr. Richard E. Edelmann, Dr. Mark P. S. Krekeler
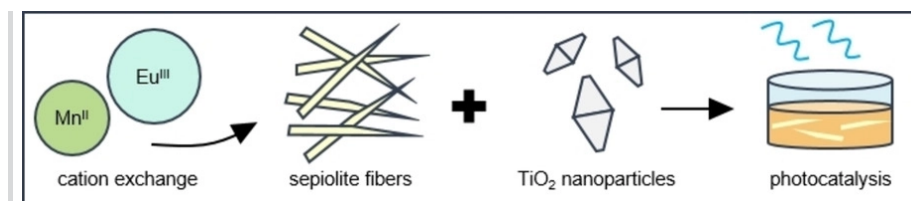
Nanocomposite photocatalysts consisting of titanium dioxide nanoparticles grown in-situ on Mn^{II}- or Eu^{III}-exchanged sepiolite fibers were fabricated and tested in ultraviolet-assisted degradation of Orange G. We have confirmed this two-step fabrication process results in unpredictable dopant migration and results in suboptimal hole (h$^+$) and superoxide ($\cdot$O$_2^-$) production and transport.

Abstract | Full text | PDF | References | Request permissions
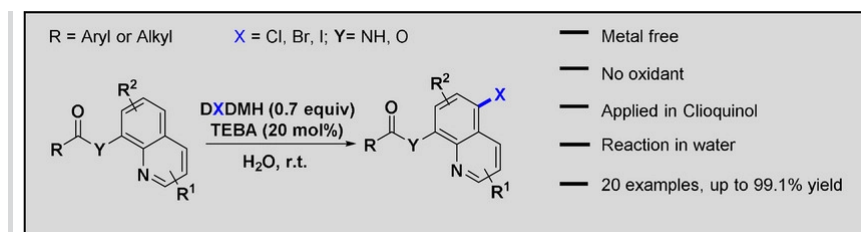

Communications

Sustainable Chemistry

Direct Phase-Transition Catalysed Monohalogenation of 8-Amidoquinolines at C5 Position in Water

Dr. Xin He, Yujia Jiang, Dr. Haiping Zhou, Dr. Qihua Zhu

This protocol provided a convenient strategy to halogenation of 8-amidoquinolines at C5 position using dihalogenated hydantoin as halogen under aqueous condition, promoted by phase-transition catalyst, affording desired products with moderate to excellent yield (20 examples, up to 99.1 % yield). This process was featured with metal-free, no oxidant and performed in water and room temperature, especially, it could be applied in Clioquinol production.

Abstract | Full text | PDF | References | Request permissions

---

Full Papers

Catalysis

Copper(I)-Catalyzed Cascade Cyclization to the Total Synthesis of Hexahydropyrroloindole Alkaloids: Flustramine B and Debromoflustramine B

Xianfu Shen, Tianfeng Peng, Fan Wang, Shumin Li, Xingfu Lei, Yunxiao, Wang, Feixiang Cheng, Teng Liu
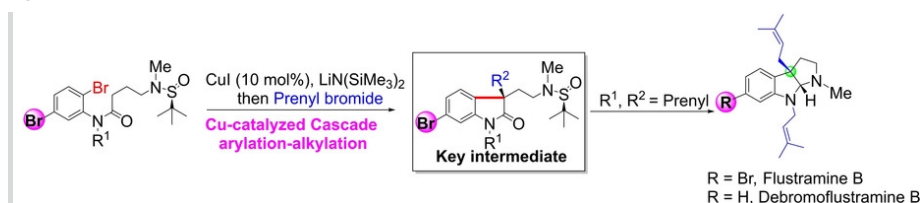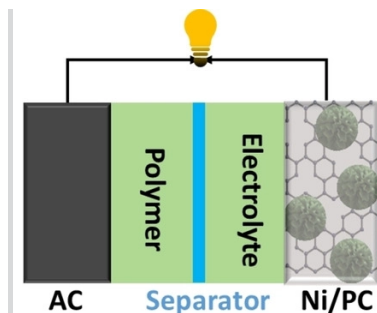
Copper(I)-Catalyzed Cascade Cyclization to the Total Synthesis of Hexahydropyrroloindole Alkaloids: Flustramine B and Debromoflustramine B In this work, we have accomplished the total synthesis of two bioactive hexahydropyrroloindole (HPI) alkaloids bearing a C3a tetrasubstituted stereocenters substituted by isopentenyl. Our route was based on Cu-catalyzed cascade arylation-

alkylation sequence in one-pot as a key step, providing Flustramine B and Debromoflustramine B with 9 steps in 37.6 % and 31.1 % overall yields, respectively.

Abstract | Full text | PDF | References | Request permissions

Organic & Supramolecular Chemistry

Copper-Catalyzed Sonogashira-Cross-Coupling of Phenols Using Dichloroimidazolidinedione

Negin Hosseini, Dr. Javad Mokhtari, Prof. Issa Yavari

Pages: 5198-5202 | First Published: 01 June 2021

In the present work phenols derivatives were activated by dichloroimidazolidinedione (DCID) and the resulting MCIDlated phenols used in the sonogashira cross-coupling for the first time. MCIDlated phenols reacted efficiently with different substituted phenyl acetylenes, the electronic and steric effects on the yields was examined in this reaction system and phenols with electron-donating groups in para, ortho and metha position and disubstituted phenols furnished the products in good yields (65–78 %).

Abstract | Full text | PDF | References | Request permissions

Materials Science inc. Nanomaterials & Polymers

Experimental Study of Poly(1-Acetamide-3-vinylimidazolium Bromide) as a Corrosion Inhibitor for N80 Carbon Steel in HCl

Minjian Kong, Prof. Yan Meng, Dr. Lei Fan, Prof. Chengxian Yin, Prof. Qibin Chen, Prof. Honglai Liu

Pages: 5203-5210 | First Published: 01 June 2021

Corrosion behaviors of poly(1-acetamide-3-vinylimidazolium bromide) (PCVIB) towards carbon steel in HCl media were studied. PCVIB is an excellent inhibitor for carbon steel, exhibiting the maximum anticorrosive efficiency of 95.8 % at the concentration of 300 ppm at 25.0 °C. PCVIB have a greater inhibition efficiency to carbon steel due to inhibitive films formed on the metal surface confirmed by the surface analysis.

Abstract | Full text | PDF | References | Request permissions

Inorganic Chemistry

Monoprotonated Dimethyl Sulfoxide, [HOSMe$_2$]$^+$: Synthesis, Crystal Structure, Spectroscopic and Theoretical Studies of [HOSMe$_2$]$_2$[OsCl$_6$] · 2H$_2$O

Dr. Olga V. Rudnitskaya, Tatiana A. Tereshina, Dr. Ekaterina V. Dobrokhotova, Dr. Ekaterina K. Kultyshkina, Dr. Alexander S. Novikov, Dr. Alexander G. Tskhovrebov, Prof. Yan V. Zubavichus, Prof. Victor N. Khrustalev

Pages: 5211-5217 | First Published: 01 June 2021

We synthesized a novel osmium complex [H(dmso)]$_2$[OsCl$_6$] · 2H$_2$O that contains a rare hydroxy(dimethyl)sulfonium cation, which is essentially the monomeric form of DMSO protonated at the oxygen atom. The crystal structure of the compound reveals a unique pattern of intermolecular bonding providing the very first example of protonated DMSO acting as S- and O-chalcogen bond donor simultaneously.

Abstract | Full text | PDF | References | Request permissions

ChemistryViews.org Home

Build Your Own Microscope

29 Jun 2021
Easy-to-build microscope achieves sub-micron resolution

Electrochemical Nitrogen Reduction on Mo$_5$N$_6$

29 Jun 2021
Reaction mechanisms of nitrogen fixation on molybdenum nitride studied

Jute in Nanotechnology Applications

28 Jun 2021
Sustainable source of nanocellulose, nanolignin, and nanocarbon materials

Rare-Earth Element Recovery from Coal Combustion Residue

28 Jun 2021
Recyclable ionic liquid used to extract coal fly ash

Directed C–H Hydroxylation with O$_2$

27 Jun 2021
Palladium complex with a bidentate pyridine-pyridone ligand as an efficient catalyst

ACES Asian Chemical Editorial Society

Sustainable Chemistry

Decorating Flower-Like Ni(OH)$_2$ Microspheres on Biomass-Derived Porous Carbons for Solid-State Asymmetric Supercapacitors

Yanfang Yang, Long Li, Baxi Luosang, Menglin Shao, Dr. Xiaoqi Fu

Pages: 5218-5224 | First Published: 01 June 2021

Flower-like Ni(OH)$_2$ microspheres decorated on biomass-derived porous carbons (Ni/PC) were used as the electroactive material with an excellent specific capacitance of 1960 F g^{-1} at 1 A g^{-1} current density. The home-assembled Ni-0.3/PC//AC solid-state asymmetric device exhibited a high energy density of 40 Wh kg^{-1} at 800 W kg^{-1} power density with superior cycle stability.

Abstract | Full text | PDF | References | Request permissions

Reviews

Catalysis

Aqueous-Phase Photocatalytic Degradation of Emerging Forever Chemical Contaminants

Prof. Dr. John N. Kuhn, Dr. Yetunde Oluwatosin Sokefun

Pages: 5225-5240 | First Published: 01 June 2021

Like diamonds, some chemicals are forever. And there is no golden bullet to purified water. This review revisits basics of heterogeneous photocatalysis for organic contaminant removal in water and then focuses on emerging, organic contaminants labeled "forever chemicals" due to persistence (long halflives, ~2+ years). The selected classes of materials are (micro)-plastics, per- and polyfluoroalkyl substances (PFAs), siloxanes, and dioxanes. Additional progress is needed for removal and destruction of these contaminants.

Abstract | Full text | PDF | References | Request permissions

Full Papers

Catalysis

🔓 Free to Read

From Single Metal to Bimetallic Sites: Enhanced Higher Hydrocarbons Yield of CO$_2$ Hydrogenation over Bimetallic Catalysts

Yu Cui, Dr. Lisheng Guo, Weizhe Gao, Kangzhou Wang, Heng Zhao, Yingluo He, Dr. Peipei Zhang, Dr. Guohui Yang, Dr. Noritatsu Tsubaki

Pages: 5241-5247 | First Published: 01 June 2021
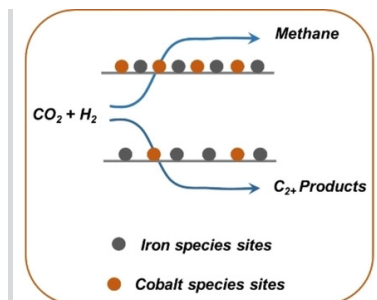
The introduction of cobalt metal into Fe-based catalyst to form a bimetallic catalyst can obviously promote the CO$_2$ hydrogenation catalytic performance. And the surface content and density of cobalt and iron can regulate the catalytic performance between methanation reaction and carbon chain propagation reaction.

Abstract | Full text | PDF | References | Request permissions

Analytical Chemistry

Fluorometric Detection of Streptavidin with a Cationic Conjugated Polymer and Hairpin DNA Probe

Ying Yan, Tingting Hu, Dr. Xinying Xiang, Dr. Wenkai Li, Dr. Changbei Ma
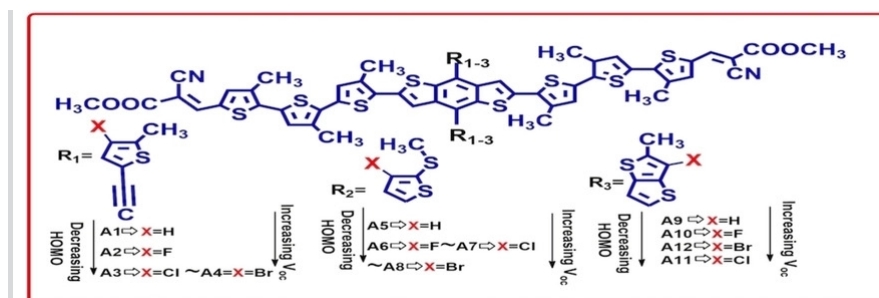
A new fluorescence strategy for streptavidin (SA) detection is developed based on a cationic conjugated polymer-mediated fluorescence resonance energy transfer (FRET). An efficient FRET from poly [(9,9-bis(6'-N, N, N-trimethylammonium) hexyl) fluorenylene phenylene (PFP) to SYBR Green I (SG I) is achieved in the presence of SA and an amplified fluorescence signal can be detected. This method has good sensitivity and specificity for SA detection.

Abstract | Full text | PDF | References | Request permissions

---

Materials Science inc. Nanomaterials & Polymers

Halogenation of the Side Chains in Donor-Acceptor Based Small Molecules for Photovoltaic Applications: Energetics and Charge-Transfer Properties from DFT/TDDFT Studies

Mohd Shavez, Anuj Kumar Ray, Prof. Aditya N. Panda

A computational study was conducted to understand the effect of halogen substitution at lateral side chains of small molecule donors. Starting with three experimentally prepared small molecule donors, we designed nine new halogenated molecules. In addition to examining the structural and optical properties, charge-transfer and charge-recombination rates are also calculated.

Abstract | Full text | PDF | References | Request permissions

---

Communications

Materials Science inc. Nanomaterials & Polymers

🔓 Open Access

Optical UV Dosimeters Based on Photoracemization of (*R*)-(+)-1,1'-Bi(2-Napthol) (BINOL) within a Chiral Nematic Liquid Crystalline Matrix

Dr. Pascal Cachelin, Dr. Hitesh Khandewal, Dr. Michael G. Debije, Prof. Ton Peijs, Prof. Cees W. M. Bastiaansen

A novel sensor involving the racemization of a chiral dopant within a nematic liquid crystalline matrix is described. The suitability of these sensors to act as personal UV dosimeters is explored. It is shown that these sensors respond to UV light with a significant change in the position of the reflection band of the chiral nematic liquid crystal, making them of interest as low-cost wearable or portable sensors for monitoring solar UV exposure.

Abstract | Full text | PDF | References | Request permissions

---

Catalysis

Ag@TiO$_2$ as an Efficient Electrocatalyst for N$_2$ Fixation to NH$_3$ under Ambient Conditions

Xue Li, Yang Cao, Tong Xu, Yonglan Luo, Dr. Tingshuai Li, Dr. Haitao Zhao, Dr. Siyu Lu, Dr. Xifeng Shi, Prof. Abdullah M. Asiri, Prof. Jianming Hu, Qian Liu, Prof. Xuping Sun

Pages: 5271-5274 | First Published: 01 June 2021
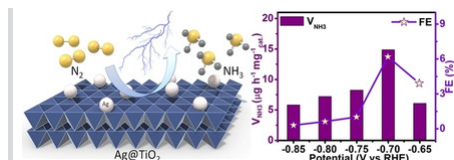
Ag composited with TiO_2 (Ag@TiO_2) can greatly improve the N_2 reduction reaction performance of TiO_2 toward ambient conversion. In 0.1 M Na_2SO_4 (pH=7), such electrocatalyst achieves a large NH_3 yield rate of 14.88 µg h^{-1} mg$^{-1}_{cat.}$ with a Faradaic efficiency of 6.2 % at −0.70 V vs. reversible hydrogen electrode. Besides, it also demonstrates high electrochemical and structural stability for NH_3 generation.

Abstract | Full text | PDF | References | Request permissions

---

Full Papers

Analytical Chemistry

A Dicyanocarbazolylstilbene-Derived Two-Photon Fluorescence Probe for Lipid Raft with a Large Two-Photon Action Cross Section

Prof. Dr. Chibao Huang, Dr. Shuai Kang, Qi Pan, Guoling Lv

Pages: 5275-5280 | First Published: 01 June 2021
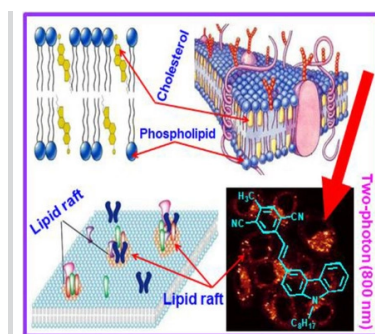
Because of such common features as a lipophilic long carbon chain, one five-membered ring and three six-membered rings, and planar-rigid molecule, DLR is able to well recognize lipid rafts and image the distribution of lipid rafts in cells and tissues, and its two-photon action cross section ($\Phi\delta$) is the largest among the reported two-photon fluorescence probes for lipid raft.

Abstract | Full text | PDF | References | Request permissions

---

Anticorrosion Inhibition Behavior of *Rhus Pentaphylla* Fruit Extracts in (1 M) HCl against Carbon Steel and their Chemical Characterization using HPLC-MS-ESI

Hajer Fadhil, Farouk Mraihi, Daoiya Zouied, Malika Trabelsi Ayadi, Jamila Kalthoum Cherif

Pages: 5281-5289 | First Published: 01 June 2021
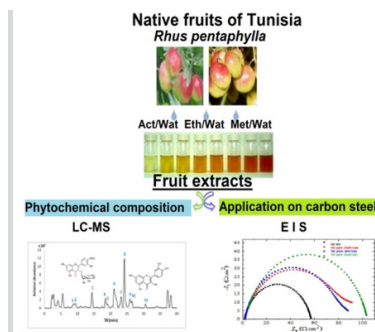
Phytochemical composition of Tunisian *R.pentaphylla* fruits during two maturity stages is investigated by LC-MS. Analysis highlighted the presence of 11 phenolic compounds. Corrosion inhibition efficiency of extracts was analyzed by polarization curves and electrochemical impedance. The extracts act as a mixed inhibitor and the electrochemical behavior analysis of carbon steel in HCl medium showed a maximum inhibition efficiency of 45.49 % with 100 ppm of the inhibitor. The results confirm the correlation between the phytochemical composition and corrosion inhibition capacity.

Abstract | Full text | PDF | References | Request permissions

---

Catalysis

An Expedient Route to Diaryl Tetrahydropentalenedione Derivatives via Intramolecular Pauson- Khand Carbonylative Cycloaddition- Oxidation Protocol

Abhijit Nayak, Manas Bandyopadhyay, Dr. Deepak Chopra, Dr. Mrinal K. Bera

Pages: 5290-5294 | First Published: 01 June 2021
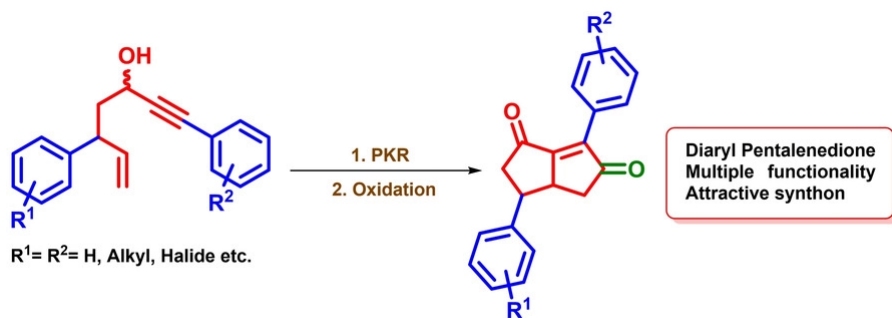
- **Good overall yield** - **Broad substrate scope** - **Operational simplicity**

3,6-diaryl tetrahydropentalene-1,5-dione, a new class of compounds have been accomplished via Pauson-Khand carbonylative cyclization-oxidation protocol. Operational simplicity, overall good yield and broad substrate scope make this method more appealing. Moreover, multiple functional groups present in the end product may be used as tool for creating complex molecular architecture such as triquinane skeleton.
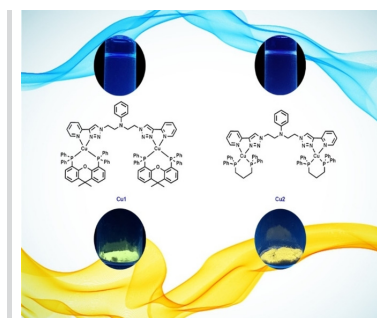
Abstract | Full text | PDF | References | Request permissions

---

Inorganic Chemistry

Three Luminescent Dinuclear Copper(I) Complexes with P^N Ligands: Synthesis, Photophysical Properties, DFT Calculations and AIE Behavior

Shao-Bin Dou, Lu Xiao, Fan Li, Yi-Zheng Zhang, Xue Lu, Jian-Ming Yang, Jie Yang, Min Wu, Dr. Zhi-Gang Niu, Prof. Gao-Nan Li

Pages: 5295-5301 | First Published: 07 June 2021

In this paper, three new dinuclear copper(I) complexes (Cu1–Cu3) were synthesized, which are based on N,N-diethylaniline-bridged triazol-pyridine (BPTA) as the N N ligand and bisphosphine ligands (Xantphos, Dppp and Binap) as the P P ligand. Their photophysical properties, theoretical calculations and aggregation induced emission (AIE) behavior were studied.

Abstract | Full text | PDF | References | Request permissions

---

Energy Technology & Environmental Science

🔓 Free to Read

Self-Assembled Au/TiO$_2$ Composite Photo-Anode Film for Highly Efficient Dye-Sensitized Solar Cells

Xiaoyan Xi, Prof. Xiangrong Ma, Ying Gong, Shiqing Bi, Prof. Hanying Wang

Pages: 5302-5306 | First Published: 07 June 2021
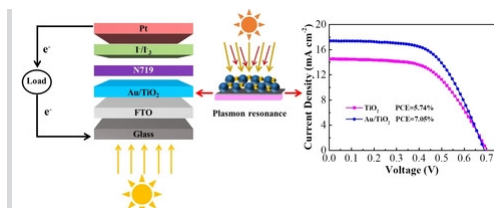
A composite Photo-anode of Au/TiO$_2$ was fabricated using facile self-assembly method. The light harvesting abilities of plasmonic DSSCs was enhanced by SPR effects. A superb overall photo-to-current conversion efficiency of 7.05 % was obtained and Au/TiO$_2$ based DSSC showed almost no loss of stability.

Abstract | Full text | PDF | References | Request permissions

---

Medicinal Chemistry & Drug Discovery

Synthesis and Molecular Docking Studies of Potent Urease Inhibitors Based on Benzoxazole Scaffold

Prof. Musa Özil, Özge Tuzcuoğlu, Dr. Nimet Baltaş, Dr. Mustafa Emirik

Pages: 5307-5312 | First Published: 07 June 2021

The series namely (2-(benzo[d]oxazol-2-ylthio)-1-(4-substitute-phenyl)ethan-1-one oxime was synthesized by the reaction of 2-aminophenol with different kinds of intermediates in several steps through both conventional and microwave techniques. All compounds were found to have an excellent degree of urease inhibitory potential ranging between 0.46±0.01 and 46.10±0.45 μM when compared with standard inhibitor acetohydroxamic acid with IC$_{50}$ 320.70±4.24 μM.
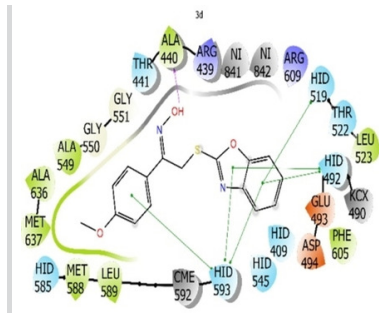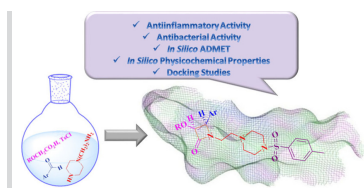
Sulfonamide-β-lactam Hybrids Incorporating the Piperazine Moiety as Potential Antiinflammatory Agent with Promising Antibacterial Activity

Dr. Roghayeh Heiran, Prof. Aliasghar Jarrahpour, Dr. Elham Riazimontazer, Dr. Ahmad Gholami, Dr. Azza Troudi, Dr. Carole Digiorgio, Prof. Jean Michel Brunel, Prof. Edward Turos

Pages: 5313-5319 | First Published: 07 June 2021

Some newly sulfonamide-*β*-lactam hybrids incorporating the piperazine moiety were synthesized and their biological activities were evaluated. Two derivatives demonstrated a similar therapeutic ratio to dexamethasone. Four derivatives showed good antibacterial activity against either E. coli and S. aureus in comparison with ampicillin as a standard, and all compounds showed low cytotoxicity towards HepG2 cell line. Moreover, molecular docking analysis supported the *in vitro* results.

Reviews

Catalysis

Triflic Anhydride (Tf$_2$O): An Efficient Catalyst for Electrophilic Activation of Amides

Zahra Tashrifi, Mohammad Mohammadi-Khanaposhtani, Bagher Larijani, Mohammad Mahdavi

Pages: 5320-5328 | First Published: 07 June 2021
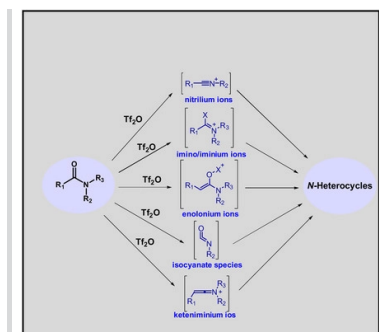
In this review, the latest research on the electrophilic activation of amides by Tf$_2$O is summarized and classified according to the the type of intermediates produced into five main categories such as: enolonium, imino/iminium, nitrilium and keteniminium ions and isocyanate species.

Full Papers

Materials Science inc. Nanomaterials & Polymers

Activity Maintenance Characteristics and Protease Adsorption on Langmuir Monolayer of Organo-Modified Single-Walled Carbon Nanotubes

Ahmed A. Almarasy, Yuna Yamada, Yuki Mashiyama, Haruka Maruyama, Yusuke Kimura, Dr. Atsuhio Fujimori

Pages: 5329-5337 | First Published: 07 June 2021

The activity maintenance characteristics of proteases adsorbed and immobilized on a monolayer of organo-modified single-walled carbon nanotubes (SWCNTs) were evaluated in this study. Activity was expected to be maintained if the biomolecules were adsorbed at low density and their three-dimensional structure could be maintained. The protease-adsorbed organo-SWCNT multilayers were immersed in an aqueous solution of luminescent casein, and fluorescence emission was observed.
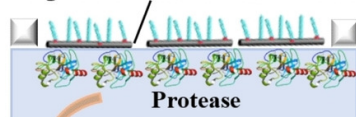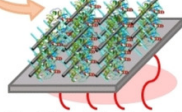
Abstract | **Full text** | **PDF** | **References** | **Request permissions**
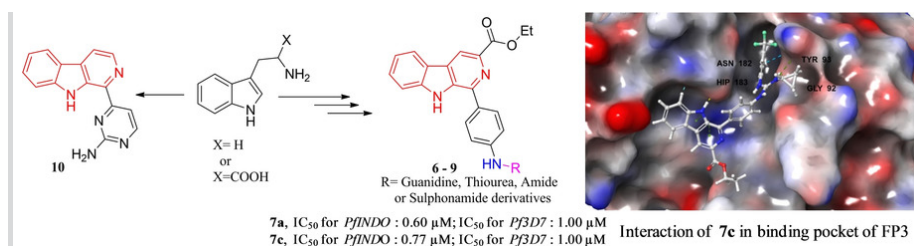

Communications

Medicinal Chemistry & Drug Discovery

In Vitro and In Silico Anti-plasmodial Evaluation of Newly Synthesized β-Carboline Derivatives

Vipin Kumar, Cheryl Sachdeva, Kamran Waidha, Dr. Sunil Sharma, Dr. Devalina Ray, Dr. Naveen Kumar Kaushik, Dr. Biswajit Saha

Pages: 5338-5342 | First Published: 07 June 2021

In this manuscript we explored the *anti*-plasmodial activity of newly synthesized β-carboline compounds conjugated with thiourea, guanidine, sulphonamide, amide and pyrimidine moiety. We successfully found two active compounds **7** a and **7** c which shows IC_{50} in micromolar range against 3D7 and INDO strain of *plasmodium falciparum*. This study will provide a great importance in future for finding lead compound against malaria.

Abstract | **Full text** | **PDF** | **References** | **Request permissions**

Full Papers

Catalysis

Evaporation-Induced Self-Assembly Method Route to TiO_2−SiO_2 Catalysts with Hierarchical Pores and Their Oximation of Ketones and Aldehydes

Dr. Fanqing Li, Dr. Zhiwei Zhou, Dr. Juan Qin, Dr. Chuanfa Liu, Dr. Yangyang Liu, Dr. Binbin He, Dr. Guangbo Xia, Prof. Wenliang Wu

Pages: 5343-5349 | First Published: 07 June 2021
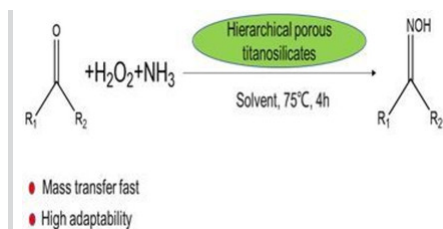
The titanosilicates with higher titanium species and hierarchical pores were prepared by an evaporation-induced self-assembly (EISA) method when tetrapropylammonium hydroxide (TPAOH) and cetyltrimethylammonium bromide (CTAB) as templates, which would be resulted in the improvement of catalytic efficiency and stability than the classical TS-1 zeolite in the oximation of ketones and aldehydes owing to the acceleration for the mass transfer efficiency of substrates.
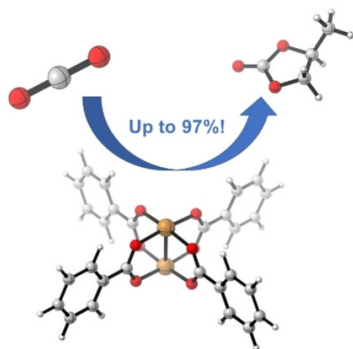
Abstract | **Full text** | **PDF** | **References** | **Request permissions**

Solvent-Free CO_2 Fixation Reaction Catalyzed by MOFs Composites Containing Polycarboxylic Acid Ligands

Yihan Tang, Wang Chen, Ruoxi Liu, Leyao Wang, Yating Pan, Ruimin Bi, Prof. Xuejun Feng, Prof. Mingyang He, Prof. Qun Chen, Prof. Zhihui Zhang

Pages: 5350-5355 | First Published: 07 June 2021

A solvent-free CO_2 fixation reaction catalyzed by copper-MOFs composites was reported, which makes yields highly up to 97 %. Theses MOFs were based on polycarboxylic acid ligands. After five catalytic cycles, the yield could remain above 90 %. Computational chemistry was applied to explain that catalytic process. After adding the catalyst, the energy barrier of the initial step of the reaction was effectively reduced.
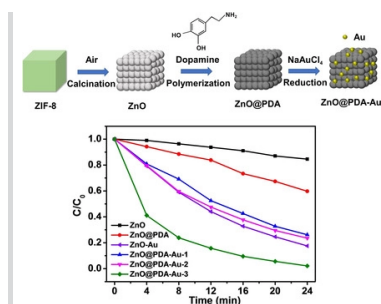
ZIF-8 Derived ZnO Decorated with Polydopamine and Au Nanoparticles for Efficient Photocatalytic Degradation of Rhodamine B

Zijun Zhang, Mei Li, Dr. Hua Wang

Pages: 5356-5365 | First Published: 07 June 2021

A new kind of composite photocatalysts was successfully synthesized through a sequential process of calcinating ZIF-8, assembling polydopamine (PDA) and reducing Au precursor. ZnO@PDA-Au-3 exhibited the highest degradation rate of 99 % within 24 min under UV-vis light irradiation, while ZnO@PDA and ZnO displayed degradation rate about 40 % and 16 %, respectively. Au played a crucial role in the enhancement of the photocatalytic performance.
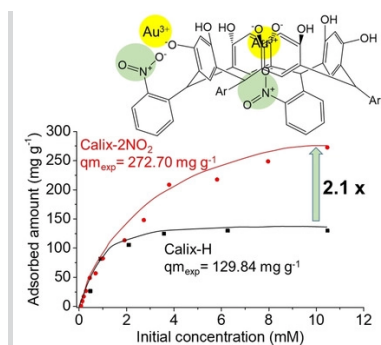
Organic & Supramolecular Chemistry

The Role of a Nitro Substituent in *C*-Phenylcalix[4]resorcinarenes to Enhance the Adsorption of Gold(III) Ions

Krisfian Tata Aneka Priyangga, Yehezkiel Steven Kurniawan, Dr. Leny Yuliati

Pages: 5366-5373 | First Published: 07 June 2021

Nitro-substituted *C*-phenylcalix[4]resorcinarene at ortho position (Calix-2NO$_2$) gave a remarkable higher adsorption capacity for gold(III) ions than the non-substituted one (Calix-H). The gold(III) ions interacted with both hydroxyl and nitro groups as well as aromatic rings of *C*-phenylcalix[4]resorcinarene through electrostatic and cation-π interactions. Such supramolecular interactions promoted the strong adsorption of gold(III) ions on the Calix-2NO$_2$. Reusability test demonstrated that the Calix-2NO$_2$ is a potential adsorbent to be used for gold(III) ions recovery.